

Characterizing the Slow Dynamics of the Swap Monte Carlo Algorithm

Published as part of *The Journal of Physical Chemistry B special issue "Mark Ediger Festschrift"*.

Kumpei Shiraishi and Ludovic Berthier*



Cite This: *J. Phys. Chem. B* 2024, 128, 12279–12291



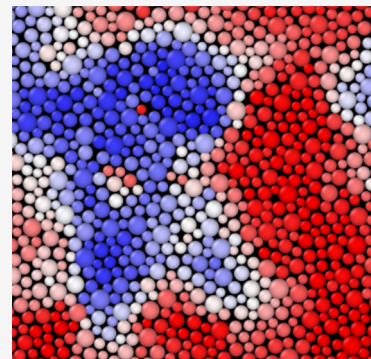
Read Online

ACCESS |

Metrics & More

Article Recommendations

ABSTRACT: The swap Monte Carlo algorithm introduces nonphysical dynamic rules to accelerate the exploration of the configuration space of supercooled liquids. Its success raises deep questions regarding the nature and physical origin of the slow dynamics of dense liquids and how it is affected by swap moves. We provide a detailed analysis of the slow dynamics generated by the swap Monte Carlo algorithm at very low temperatures in two glass-forming models. We find that the slowing down of the swap dynamics is qualitatively distinct from its local Monte Carlo counterpart, with considerably suppressed dynamic heterogeneity at both single-particle and collective levels. Our results suggest that local kinetic constraints are drastically reduced by swap moves, leading to nearly Gaussian and diffusive dynamics and weakly growing dynamic correlation length scales. The comparison between static and dynamic fluctuations shows that swap Monte Carlo is a nearly optimal local equilibrium algorithm, suggesting that further progress should necessarily involve collective or driven algorithms.



I. INTRODUCTION

When glass-forming liquids are cooled, molecular motion becomes very slow while their structure remains disordered; they eventually become glasses.¹ The glass transition is an important research subject that has been studied over many years using both experiments and theory.^{1,2} Numerical studies are vitally important because simulations can provide complete information about microscopic particle motion near the glass transition.³ However, computational studies of the glass transition are inherently difficult. Close to the transition, slow molecular motion results in rapidly growing relaxation times, and equilibrium sampling of the configuration space becomes difficult within reasonable CPU times. At low temperatures, conventional molecular dynamics (MD)⁴ or local Monte Carlo (MC)^{5,6} methods become inefficient. To achieve sampling near the experimental glass transition, various enhanced techniques have been implemented.⁷ For instance, the parallel tempering method allows a faster exploration of the rugged free energy landscape.^{8–10} Instead, event-chain and lifted Monte Carlo algorithms propose collective particle moves to improve the local Metropolis Monte Carlo approach.^{11–14} Recently, machine learning techniques were also applied to sample low-temperature configurations.^{10,15} Despite good progress, none of these methods has been able to provide substantial improvement over conventional MD and MC techniques so far.

For certain models of supercooled liquids, the swap Monte Carlo (SMC) method^{16,17} completely changes the situa-

tion.^{18,19} In recent years, the SMC algorithm has attracted significant attention, leading to the development of several continuous or discrete polydisperse particle models optimized for this method.^{19–23} In such models, SMC is remarkably efficient, accelerating relaxation processes by more than 10 orders of magnitude, compared to local MC and MD methods. Therefore, it has become possible to access very low temperature regimes that were previously inaccessible. Various aspects of glass physics were then investigated, such as thermodynamics,^{20,24,25} plasticity,^{26,27} thermal vibrations,²⁸ and two-level systems.^{29,30} Additionally, this technique allows for in-silico generation of particle configurations with stability comparable to the one achieved experimentally by physical vapor deposition,^{31,32} thus offering useful insights into the physics of ultrastable glasses.^{33–36}

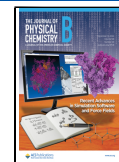
Thanks to SMC, new insights were also gathered regarding the low-temperature relaxation processes in supercooled liquids.³⁷ It has long been known that the relaxation of liquids near the glass transition is spatially heterogeneous.^{38–41} By allowing numerical studies at much lower temperatures and

Received: October 3, 2024

Revised: November 13, 2024

Accepted: November 14, 2024

Published: December 1, 2024



longer times, SMC was used to clarify the relative role of rare activation events and dynamic facilitation⁴² in the formation of dynamic heterogeneity in model supercooled liquids.^{37,43–45}

Surprisingly, no such detailed real-space characterization of relaxation processes is available for the dynamics produced by SMC itself, which also becomes slow at low temperatures. This gap is presumably explained by the nonphysical nature of the particle swaps introduced by SMC, which makes the Monte Carlo dynamics somewhat artificial. However, several explanations proposed to account for the success of SMC all make assumptions and predictions about the influence of particle swaps on the relaxation dynamics that have not been tested directly. In particular, the role of local kinetic constraints,^{46–48} dynamic facilitation and activated processes,⁴⁹ the existence of a shifted mode-coupling crossover temperature^{50–52} were invoked. It would be desirable to connect these theoretical discussions with detailed real-space characterization of the relaxation processes generated by the SMC dynamics. Such analysis could also provide useful guidance in the context of recent attempts to improve SMC by incorporating event-driven and collective swap moves.^{13,14}

Here, we characterize the slow dynamics and its spatial and temporal heterogeneity in SMC dynamics by performing simulations of two glass-forming models, in which SMC provides a very large acceleration of the dynamics. We characterize the dynamic heterogeneity at the single-particle and collective levels, emphasizing differences and similarities with the physical dynamics obtained using conventional MC. We find that the dynamic heterogeneity in SMC dynamics is much weaker and the relaxation is spatially more homogeneous. Interestingly, the dynamic length scale controlling the SMC dynamics is very close to the static point-to-set length scale, which governs thermodynamic fluctuations associated with the approach to a random first-order transition.^{53–55} This suggests that, for the studied models, SMC is an almost optimal local equilibrium algorithm.

The manuscript is organized as follows. In **Section II**, we present the two models and numerical methods used. In **Section III**, the bulk relaxation is characterized for normal MC and SMC. We then characterize the dynamic heterogeneity of the relaxation. In **Section IV**, we present indicators of dynamic heterogeneity at the single-particle level, while **Section V** characterizes the collective behavior of the relaxation and its relation to static quantities. In **Section VI**, we quantify the correlation between the MC and SMC dynamics. Finally, we conclude in **Section VII**, where we present a theoretical discussion of the numerical results and their implications.

II. MODELS AND NUMERICAL METHODS

We consider systems of continuously polydisperse particles^{19,20} enclosed in a square ($D = 2$) or cubic box ($D = 3$) with periodic boundary conditions. Two particles i and j separated by a distance r_{ij} interact via a repulsive potential

$$\nu(r_{ij}) = \epsilon \left(\frac{\sigma_{ij}}{r_{ij}} \right)^{12} + c_0 + c_2 \left(\frac{\sigma_{ij}}{r_{ij}} \right)^2 + c_4 \left(\frac{\sigma_{ij}}{r_{ij}} \right)^4 \quad (1)$$

if $r_{ij} < 1.25 \sigma_{ij}$; otherwise, the potential is zero. The constants c_0 , c_2 , and c_4 are chosen to ensure the continuity of the potential up to its second derivative at the cutoff. A nonadditive interaction rule $\sigma_{ij} = 0.5(\sigma_i + \sigma_j)(1 - 0.2|\sigma_i - \sigma_j|)$ is employed to avoid crystallization and phase separation at low temperatures.¹⁹ The diameters $\{\sigma_i\}$ of the particles are

drawn from a distribution $P(\sigma) \propto 1/\sigma^3$ in a finite range [0.73, 1.62]. The number of particles is N and the linear length L of the simulation box is determined from the number density $\rho = N/L^D = 1.0$ ($D = 2, 3$), using the average particle diameter as the unit length. In both two dimensions (2D) and three dimensions (3D), we consider systems with $N = 1000$. The temperature is expressed in units of ϵ by taking the Boltzmann constant to unity.

At each temperature T , the system is first equilibrated by the SMC method. For each MC attempt, we randomly pick up one particle i , located at \mathbf{r}_i , and move its position to $\mathbf{r}_i + \delta\mathbf{r}$, with $\delta\mathbf{r}$ being a random vector in a cube of linear length $\delta = 0.15$. In addition to translational motion, a swap move exchanging the diameters of two randomly chosen particles is also proposed with a probability of 0.2. Both types of MC proposed moves are accepted according to the Metropolis condition. We define N attempted moves as one MC step, which is our time unit. After equilibrium configurations are obtained by SMC, we perform either SMC or standard MC simulations, where no swap move occurs.

III. BULK RELAXATION DYNAMICS

III.A. Self-Intermediate Scattering Function. We start by presenting a comparison of the bulk dynamics between MC and SMC. To this end, we compute the self-intermediate scattering function

$$F_s(q, t) = \left\langle \frac{1}{N} \sum_{i=1}^N \cos(\mathbf{q} \cdot \Delta\mathbf{r}_i(t)) \right\rangle \quad (2)$$

where $\Delta\mathbf{r}_i(t) = \mathbf{r}_i(t) - \mathbf{r}_i(0)$, and the angled brackets indicate an ensemble average. The motion of the center of mass of the system is removed. The wavevectors are chosen as $q = 6.7$ in 3D,⁴³ $q = 6.5$ in 2D.²⁰ In the 2D system, we use the cage-relative displacements $\Delta\mathbf{r}_i^{CR}(t)$ (removing the motion of the center of mass of the neighbors of particle i) instead of $\Delta\mathbf{r}_i(t)$, to minimize the influence of Mermin–Wagner fluctuations.^{56,57}

In **Figure 1**, $F_s(q, t)$ is presented for both MC and SMC dynamics for temperatures ranging from $T = 0.400$ to $T = 0.060$ in the 3D system. At high temperature, $T = 0.400$, which is above the onset temperature $T_0 \approx 0.266$ in 3D,⁵⁸ $F_s(q, t)$ decays with a single relaxation step in both SMC and MC dynamics. As T is lowered, a plateau develops in $F_s(q, t)$ in the MC dynamics, and the relaxation of $F_s(q, t)$ then proceeds with the well-known two-step relaxation process.² At temperatures around and below the mode-coupling crossover temperature, $T_{MCT} = 0.107$,¹⁹ it is no longer possible to observe the entire decay of $F_s(q, t)$ within our simulation time window when using the MC dynamics. By contrast, the relaxation of SMC does not show the same slowing down observed in normal MC dynamics when lowering temperatures. The emergence of a plateau with SMC occurs at a much lower temperature, near $T \approx 0.080$, but its complete decay can easily be observed, even at temperatures much below T_{MCT} . These results agree with previous results^{19,59} and show that the dynamic relaxation is very much accelerated by the introduction of swap moves. Similar data are obtained in the 2D system (not shown). Overall, the SMC results show that a form of slow dynamics, characterized by a two-step decay of bulk correlation function, is also emerging at sufficiently low temperatures for SMC. In the remainder, we characterize this slow dynamics in detail.

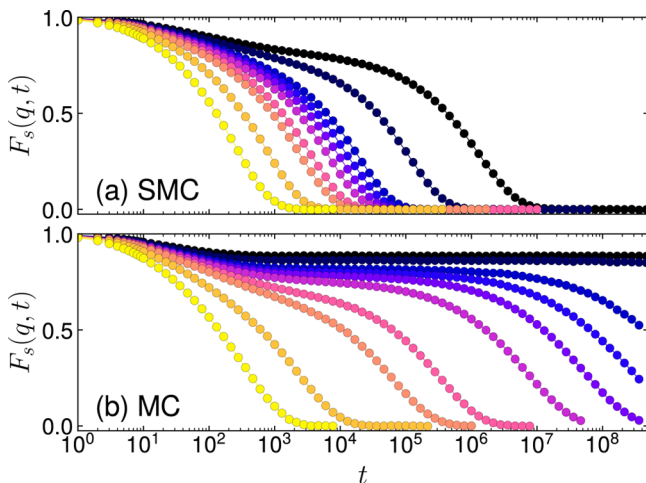


Figure 1. Self-intermediate scattering function $F_s(q, t)$ defined in eq 2 for (a) SMC and (b) MC dynamics in 3D. Each color corresponds to a temperature, with $T = 0.400, 0.200, 0.130, 0.117, 0.102, 0.095, 0.090, 0.085, 0.070$, and 0.060 , from left to right in both panels. A similar two-step decay emerges at low T in both dynamics, but SMC relaxes much faster than MC at any given T .

III.B. Structural Relaxation Time. We characterize the acceleration offered by the swap moves by measuring the structural relaxation time τ_α defined as $F_s(q, t = \tau_\alpha) = e^{-1}$. As shown in Figure 2, the structural relaxation time of SMC is

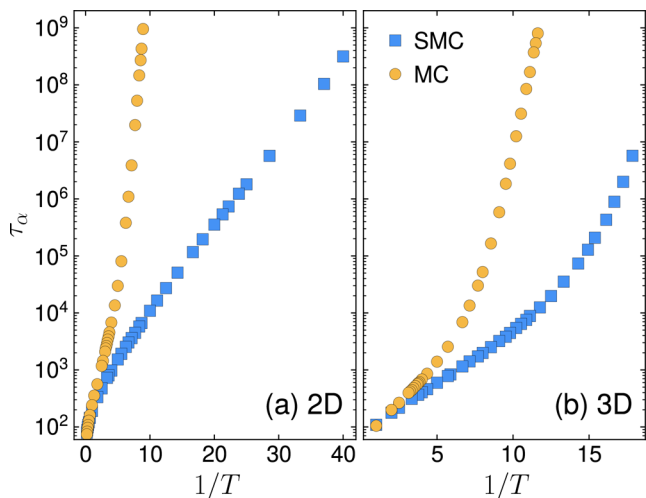


Figure 2. Temperature dependence of the structural relaxation time τ_α of SMC and MC dynamics in (a) 2D and (b) 3D.

much shorter than that of MC at each temperature. The first conclusion, known from previous work on SMC,^{19,20} is that SMC can reach thermal equilibrium at temperatures much lower than conventional MC.

Let us take a closer look at the temperature evolution of the structural relaxation times in Figure 2. In 2D, the SMC data show a nearly Arrhenius behavior down to very low temperatures, with a temperature scale that is much smaller than for MC dynamics. This leads to a very large acceleration of the relaxation dynamics.²⁰

At high temperatures in 3D, the SMC dynamics shows an Arrhenius growth of τ_α down to an onset temperature $T \approx 0.1$, which is much lower than the onset temperature for MC dynamics ($T \approx 0.25$). We can also compare the location of the

mode-coupling crossovers for both dynamics by fitting the relaxation times to a power law, $\tau_\alpha \approx (T - T_{\text{MCT}})^{-\gamma}$, as predicted by the mode-coupling theory of the glass transition.⁶⁰ We obtain $T_{\text{MCT}} = 0.144$ in 2D and $T_{\text{MCT}} = 0.107$ in 3D for MC dynamics, consistent with previous estimates.^{19,43} For the SMC dynamics, we find $T_{\text{MCT}} = 0.036$ in 2D and $T_{\text{MCT}} = 0.055$ in 3D. The quality of the fits in all cases is similar, and the power describes ~ 3 decades of the evolution of the relaxation times. These fits are consistent with a shift of the location of the mode-coupling transition by the swap moves,^{50–52,61} but given the modest quality of the fits, it is difficult to draw firm conclusions on this point.

IV. SINGLE-PARTICLE DYNAMIC HETEROGENEITY

IV.A. Van Hove Distributions. A major feature of dynamic relaxation processes near the glass transition is the presence of dynamic heterogeneity.^{38–40} This name generically refers to the existence of spontaneous fluctuations of the local dynamics with the coexistence of fast and slow regions in the material. While this is well-documented for supercooled liquids relaxing via physical dynamics such as MC⁶² and MD,^{63,64} we wish to analyze the behavior obtained from the SMC dynamics.

We start by analyzing the van Hove distribution function, which is defined as

$$P(\Delta r(t)) = \left\langle \frac{1}{DN} \sum_i \sum_\alpha \delta[\Delta r - (r_{i\alpha}(t) - r_{i\alpha}(0))] \right\rangle \quad (3)$$

where $\delta(x)$ is the Dirac delta function and $\alpha = x, y$ (and z for $D = 3$). Notice that since diameters fluctuate in time in the SMC dynamics, it makes little sense to distinguish particles by their sizes to record their dynamics.

In Figures 3 and 4, the time dependence of the van Hove function in MC and SMC is shown for 2D and 3D systems, respectively. In these figures, temperatures are chosen so that structural relaxation times τ_α are approximately the same for MC and SMC to make the comparison meaningful.

For MC dynamics, $P(\Delta r(t))$ has a Gaussian shape at short times, as expected from thermal motion within a solid. However, as time increases, the distribution develops non-Gaussian tails that signal the presence of particles that relax much faster than the bulk and start exploring large distances at times much shorter than τ_α .^{63,64} At intermediate times, the van Hove distribution appears clearly bimodal and is well-described, at least qualitatively, as the superposition of two populations of particles. Such property of single-particle displacements is well-known and universal among many glass-formers when dynamics is slow.⁶⁴ The van Hove distribution returns to a Gaussian distribution in the limit of large times only ($t/\tau_\alpha \rightarrow \infty$).⁶⁵

The data for the SMC dynamics, by contrast, show much weaker signs of non-Gaussianity. The distributions are again close to a Gaussian at short times, as observed in MC. However, as time increases, the distributions seem to broaden in a relatively homogeneous manner with no clear emergence of broad exponential tails. A clear separation between mobile and immobile particles is not observed in SMC dynamics, even as time increases toward τ_α . This observation suggests that the dynamic heterogeneity is suppressed in the SMC dynamics. The comparison between 2D and 3D data also shows that the suppression is somewhat weaker in 3D than in 2D, which

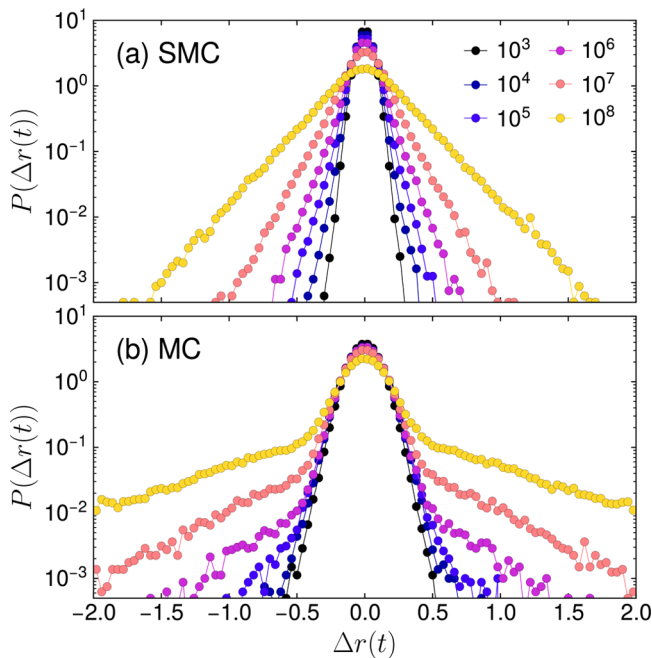


Figure 3. Van Hove distribution function at different times in 2D for (a) SMC at $T = 0.025$ where $\tau_\alpha = 3.2 \times 10^8$ and (b) MC at $T = 0.115$ where $\tau_\alpha = 4.3 \times 10^8$. The non-Gaussian nature of particle distribution observed in MC dynamics is considerably suppressed for SMC.

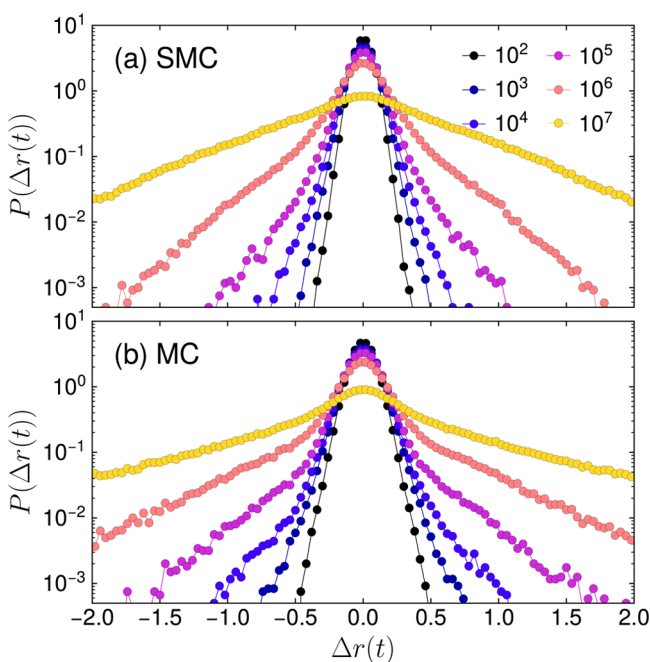


Figure 4. Van Hove distribution function at different times in 3D for (a) SMC at $T = 0.058$, where $\tau_\alpha = 2.0 \times 10^6$, and (b) MC at $T = 0.105$, where $\tau_\alpha = 1.8 \times 10^6$. The non-Gaussian nature of the particle distribution observed in MC dynamics is considerably suppressed for SMC.

correlates with the relative efficiency of the SMC equilibration speedup observed in the two models.

IV.B. Non-Gaussian Parameter. To quantitatively characterize the non-Gaussianity of the distribution, we calculate the non-Gaussian parameter $\alpha_2(t)$,⁶⁶ which is generally expressed as

$$\alpha_2(t) = \frac{D}{D + 2} \frac{\langle r^4(t) \rangle}{\langle r^2(t) \rangle^2} - 1 \quad (4)$$

in D dimensions,⁶⁷ so that $\alpha_2 = 0$ if the van Hove distribution is Gaussian.

In Figure 5a, $\alpha_2(t)$ values of SMC and MC are shown for the 2D system, for temperatures chosen to have comparable

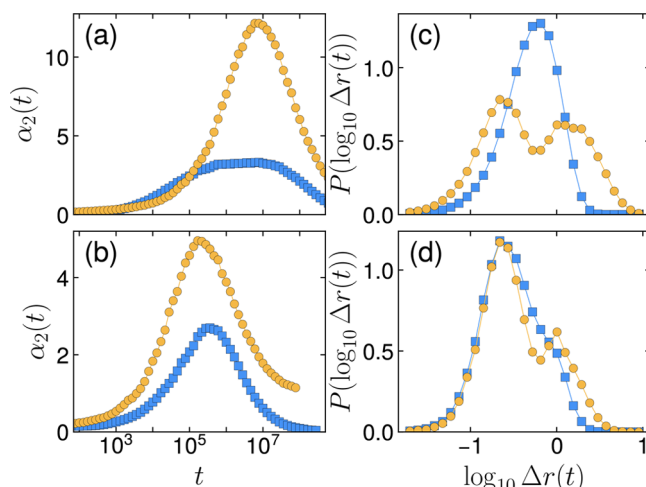


Figure 5. Non-Gaussian parameter $\alpha_2(t)$ for SMC (blue squares) and MC (yellow circles) dynamics in (a) 2D and (b) 3D. In 2D, SMC data are for $T = 0.025$ ($\tau_\alpha = 3.2 \times 10^8$) and MC data for $T = 0.115$ ($\tau_\alpha = 4.3 \times 10^8$). In 3D, SMC data are for $T = 0.058$ ($\tau_\alpha = 2.0 \times 10^6$) and MC data for $T = 0.105$ ($\tau_\alpha = 1.8 \times 10^6$). The distributions $P(\log_{10} \Delta r(t))$ in (c) 2D for $t = 4.6 \times 10^8$ and (d) 3D for $t = 1.7 \times 10^6$.

relaxation times. Both functions have the expected non-monotonic time dependence with a peak at a time about 10 times shorter than τ_α indicating maximal deviation from Gaussianity. However, the peak height is considerably lower for SMC than for MC (by a factor of ~ 3), in agreement with the distributions shown in Figure 3. A similar suppression is observed in the 3D system in Figure 5b, but the suppression is slightly smaller (by a factor of ~ 2).

As a complementary view, we present the probability distribution of the logarithm of particle displacements $P(\log_{10} \Delta r(t))$ for times near the peak of $\alpha_2(t)$. In this representation,⁶⁸ the MC dynamics displays a bimodal shape with two distinct peaks, while the SMC distributions do not. These results confirm that the drastic reduction of the non-Gaussian parameter indeed results from a weaker distinction between fast and slow particles in the relaxation processes emerging from the SMC dynamics.

Finally, we follow the temperature evolution of the peak of $\alpha_2^*(t)$, which we denote α_2^* (see Figure 6). As observed in Figure 2, both dynamics display very different relaxation times at the same temperature T . Therefore, it makes sense to compare them at equal values of the relaxation time τ_α , as we adopt in Figure 6 where the temperature is used as a parametric variable. Even in this representation, the suppression of α_2^* in the SMC dynamics remains obvious. In 3D, α_2^* starts to increase at very low temperatures for SMC, while in 2D there is no such tendency and α_2^* remains very modest down to extremely low temperatures.

Overall, we conclude from this section that the single-particle dynamics in SMC exhibits a very modest dynamic

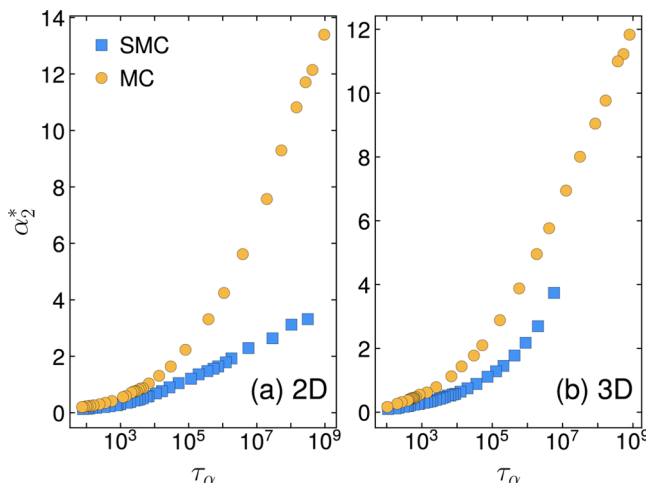


Figure 6. Temperature evolution of the peak value α_2^* of the non-Gaussian parameter for SMC and MC dynamics in (a) 2D and (b) 3D is represented using a parametric plot against the relaxation time $\tau_\alpha(T)$. The non-Gaussian parameter is strongly suppressed by the SMC dynamics, even when the two dynamics are compared at equal relaxation times, with a more spectacular suppression in 2D.

heterogeneity with a very weak contrast between fast and slow particles, leading to nearly Gaussian van Hove distributions, no broad exponential tails, and small values of the non-Gaussian parameter compared to the conventional MC dynamics.

IV.C. Decoupling between Self-Diffusion and Structural Relaxation. An important manifestation of the presence of dynamic heterogeneity in supercooled liquids is the well-documented decoupling between the self-diffusion coefficient $D_s(T)$ and the bulk viscosity $\eta(T)$.³⁸ While both quantities are related by the Stokes–Einstein relation in simple liquids, $D_s \approx T/\eta$, this relation is violated when both D_s and η vary by orders of magnitude upon approaching the glass-transition temperature. The resulting decoupling phenomenon has attracted significant attention in experimental studies^{38,69,70} as well as numerical and theoretical studies.^{71–77}

Here, we study whether decoupling is observed in SMC dynamics and compare the results with MC dynamics. To analyze the decoupling, it is more convenient to compare the temperature evolution of the self-diffusion constant defined from the mean-squared displacements, $D_s = \lim_{t \rightarrow \infty} \langle |\Delta r_i(t)|^2 \rangle / (2Dt)$, to that of the structural relaxation time $\tau_\alpha(T)$. It is known that τ_α and η have typically a similar temperature dependence.⁷⁶ For simple liquids obeying simple diffusive motion, the structural relaxation time $\tau_\alpha(q, T)$ measured at a given wavevector q and temperature T is related to $D_s(T)$ as $\tau_\alpha(q, T) \approx 1/(D_s(T)q^2)$. In this Fickian limit, the product $D_s \times \tau_\alpha$ is a constant independent of temperature.⁷⁸ We study deviations from this Fickian reference for the two models at hand.

The analysis of decoupling in Figure 7 shows the parametric evolution of D_s with τ_α as the temperature is varied. In MC dynamics, decoupling occurs, and the relation $D_s \approx \tau_\alpha^{-1}$ breaks down as temperature is lowered. A fractional relation describes the decoupling accurately, $D_s \approx \tau_\alpha^{-\zeta}$ with values of $\zeta = 0.70$ and $\zeta = 0.72$ observed in 2D and 3D, respectively, instead of the expected $\zeta = 1$ in the absence of decoupling. In agreement with the suppression of single-particle heterogeneity, we also find that decoupling is strongly suppressed for SMC dynamics in both 2D and 3D, with exponents $\zeta = 0.81$ in 3D and $\zeta = 1$ in

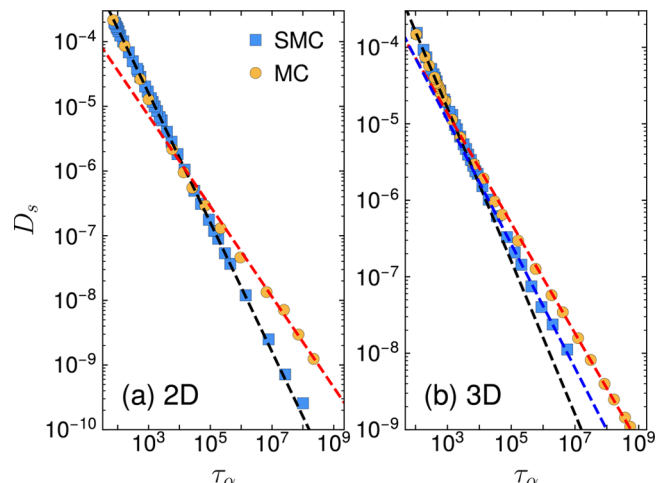


Figure 7. Structural relaxation time dependence of the self-diffusion constant D_s . The black dashed line in both panels is $D_s \approx \tau_\alpha^{-1}$. The red dashed line shows $D_s \approx \tau_\alpha^{-0.70}$ in the 2D panel and $D_s \approx \tau_\alpha^{-0.72}$ in the 3D panel. The blue dashed line in the 3D panel is $D_s \approx \tau_\alpha^{-0.81}$.

2D. Therefore, the suppression of dynamic heterogeneity is accompanied by a drastic suppression of decoupling, which is vanishingly small in 2D. We have confirmed these conclusions by analyzing the wavevector dependence of the structural relaxation time τ_α ^{72,78} and found indeed that diffusive dynamics is very nearly recovered for 2D while deviations from diffusive behavior are very small in 3D.

Finally, we briefly discuss the influence of Mermin–Wagner fluctuations on decoupling in 2D. In Figure 7, we used normal displacements $\Delta r_i(t)$ instead of cage-relative displacements $\Delta r_i^{CR}(t)$ to compute both D_s and τ_α . Employing cage-relative displacements removes the influence of Mermin–Wagner fluctuations on τ_α for relatively large wavevectors, but this correction leads to an incorrect estimate of the diffusion constant D_s .^{79,80} To avoid this artifact, we decided to use normal displacements in the D_s calculations and we chose a relatively modest system size ($N = 1000$) to reduce the influence of Mermin–Wagner fluctuations on τ_α . We have checked that a similar amount of decoupling is observed when τ_α is calculated from the cage-relative definition of $F_s(q, t)$, so that our conclusions regarding the comparison between MC and SMC are robust.

V. COLLECTIVE DYNAMICS

V.A. Four-Point Dynamic Susceptibility. The analysis of single-particle dynamics revealed that the distinction between the fastest and slowest particles is suppressed by SMC dynamics. Yet, these fluctuations do not completely vanish, and in any trajectory spontaneous dynamic fluctuations remain present. In this section, we ask whether these fluctuations are spatially correlated. For MC dynamics, a large number of studies have clarified the presence and temperature evolution of growing dynamic length scales.^{40,81} We now perform a similar analysis for SMC dynamics.

To this end, we compute the four-point dynamic susceptibility, which is the standard tool for measuring dynamic heterogeneity.^{82–85} We define the dynamic susceptibility from the spontaneous fluctuations of the instantaneous value of the self-intermediate scattering function $\hat{F}_s(q, t)$ around its average $F_s(q, t)$ in eq 2:

$$\chi_4(t) = N[\langle \hat{F}_s(q, t)^2 \rangle - \langle \hat{F}_s(q, t) \rangle^2] \quad (5)$$

By definition, we have $F_s(q, t) = \langle \hat{F}_s(q, t) \rangle$. To normalize $\chi_4(t)$, it is convenient to consider the situation where no correlation exists between particles. In that case, $\chi_4(t)$ reduces to the single-particle quantity $\chi_s^s(t) = \text{Var}(f_s^i)$, with $f_s^i = \cos(\mathbf{q} \cdot \Delta\mathbf{r}_i)$ the single-particle contribution to $F_s(q, t)$, and $\text{Var}(x) = \langle x^2 \rangle - \langle x \rangle^2$. We then define a rescaled four-point function as

$$\tilde{\chi}_4(t) = \frac{\chi_4(t)}{\chi_s^s(t)} \quad (6)$$

As defined in eq 6, $\tilde{\chi}_4(t) \approx 1$ at both very short and very long times, when interparticle correlations play no role, while the amplitude of $\tilde{\chi}_4(t)$ at intermediate times roughly reflects the volume of dynamic correlations.^{62,85}

The normalized dynamic susceptibility $\tilde{\chi}_4(t)$ for SMC dynamics in 2D and 3D is shown in Figure 8 for a broad

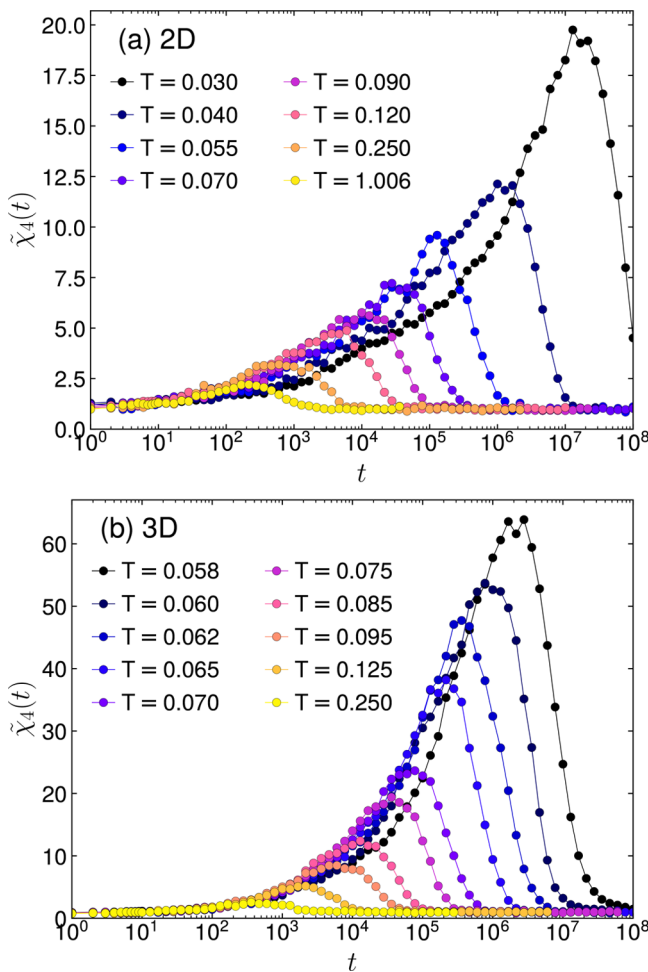


Figure 8. Time dependence of the normalized dynamic susceptibility $\tilde{\chi}_4(t)$ for the SMC dynamics in (a) 2D and (b) 3D at different temperatures.

range of temperatures. As expected, it is close to unity at both short and long times, and it develops a peak at a time scale that is dependent on the average structural relaxation time τ_α , as frequently observed for conventional MD dynamics.^{62,77,83,86,87} Importantly, the amplitude of the peak of the susceptibility increases far above unity as the temperature decreases and dynamics slows down.

The peak height of the dynamic susceptibility represents the typical volume of spatially correlated domains.⁸⁵ We denote it as $\tilde{\chi}_4^*(T)$ and present its evolution with temperature in Figure 9, where we again use a parametric representation against the average relaxation time $\tau_\alpha(T)$ to compare MC and SMC dynamics on an equal footing.

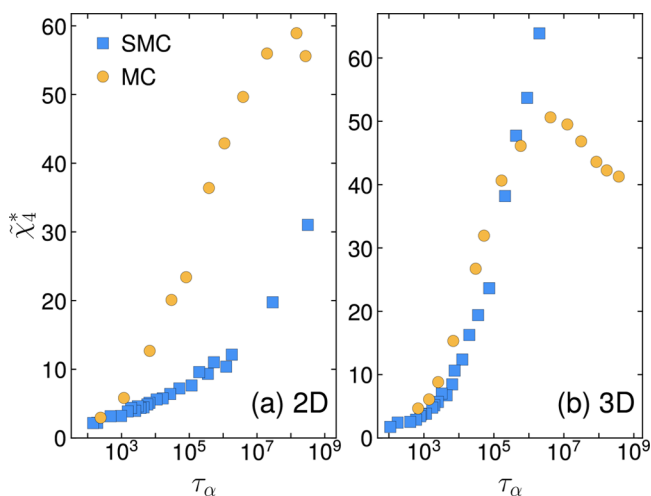


Figure 9. Parametric evolution of the peak height of the dynamic susceptibility $\tilde{\chi}_4^*(T)$, as a function of the structural relaxation time $\tau_\alpha(T)$ for both MC and SMC dynamics in (a) 2D and (b) 3D.

Starting with 3D and the MC dynamics, we observe the usual behavior where $\tilde{\chi}_4^*$ grows by lowering the temperature, but exhibits a much slower growth below the mode-coupling crossover temperature near $T_{\text{MCT}} \approx 0.107$.¹⁹ A similar crossover behavior has been widely reported before in other models of glass-forming liquids.^{77,87,88} In the SMC dynamics, $\tilde{\chi}_4^*$ evolves very similarly when represented against the relaxation time (see Figure 9b), but we observe no sign of a plateau or a saturation at the lowest studied temperature; perhaps we cannot reach as long time scales with SMC compared to MC dynamics. At low temperatures, the roughly linear relation between $\tilde{\chi}_4^*$ and $\log \tau_\alpha$ suggests that the relaxation time grows exponentially faster with the correlation volume. We note that these data can also be described with the power law $\tilde{\chi}_4^* \approx \tau_\alpha^{0.2}$, with a fairly small exponent that is often compatible with a logarithmic relation.

The comparison is again different in the 2D system. First, in the normal MC dynamics, no clear crossover to the plateau is observed, perhaps because the temperature range we observed ($T \geq 0.117$) is not much below $T_{\text{MCT}} = 0.120$. A more important difference is the comparison between the MC and SMC dynamics. While in 3D both dynamic susceptibilities grow similarly with τ_α in the 2D system, the dynamic susceptibility is much smaller both when compared at the same temperature and when compared at the same value of the relaxation time. At the longest relaxation time we could access, the dynamic susceptibility for SMC is about twice as small as the one in MC.

V.B. Dynamic and Static Correlation Length Scales.

The observation that dynamic susceptibilities have distinct values in MC and SMC dynamics at the same temperature is important, as this directly suggests that the peak value $\tilde{\chi}_4^*$ is sensitive to the microscopic dynamic rules and is therefore not uniquely controlled by static, thermodynamic, or structural

fluctuations which are, by definition, insensitive to the chosen dynamics.

Here, we discuss this point in more depth and collect a number of estimates for correlation length scales discussed before for the present models in order to understand better their interrelation, if any. To this end, we first convert the measured dynamic susceptibilities into correlation length scales using the proxy

$$\xi_d = (\tilde{\chi}_4^*)^{1/D} \quad (7)$$

thus giving us estimates for the dynamic correlation length scale ξ_d for both dynamics in both 2D and 3D. The results are shown in Figure 10, which represents the temperature evolution of the resulting dynamic length scales for both 2D and 3D.

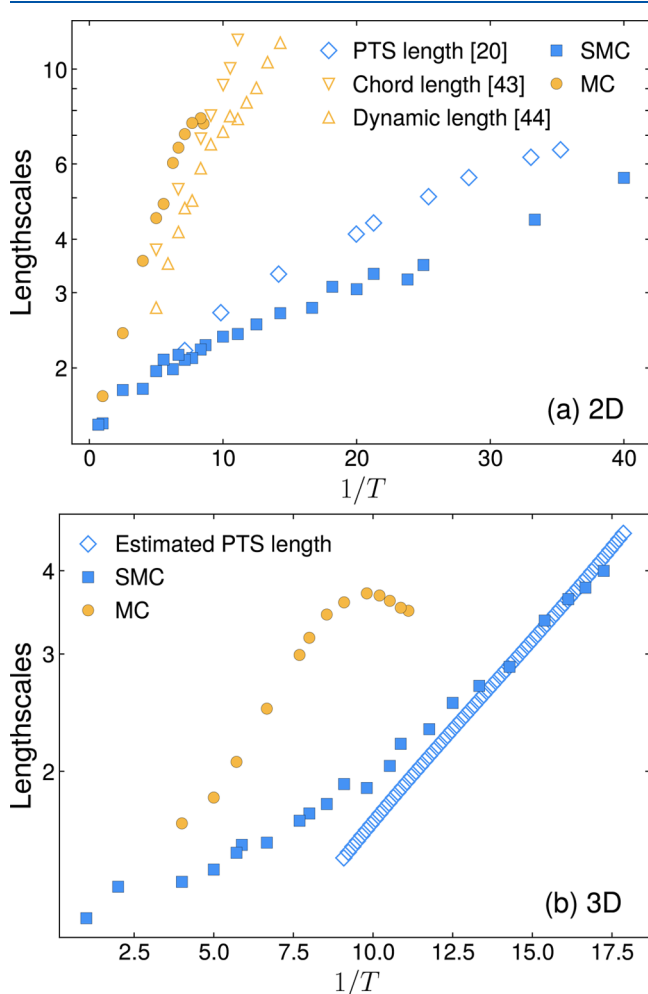


Figure 10. Temperature evolution of various estimates for static and dynamic length scales in (a) 2D and (b) 3D, using an Arrhenius representation.

In 2D, we can compare the resulting dynamic length scale to two independent estimates obtained via completely different methods: the average chord length extracted in ref 43, and the dynamic length scale obtained from the inhomogeneous geometries studied in ref 44, for the same 2D system. The data shown in Figure 10(a) show a good degree of agreement for the MC dynamics and provide a consistent trend for the

temperature evolution of the dynamic length scale characterizing the MC dynamics.

When we add the dynamic length scale estimated for the SMC dynamics using eq 7 to the same figure, we confirm that the amplitude and temperature dependence of these SMC dynamic correlation length scales are totally different than the three dynamic length scales obtained from MC dynamics. The SMC dynamic correlations are much shorter-ranged, and grow slower with decreasing temperature. This decoupling between the two types of correlation length scales indicate that they have a different physical origin and, in particular, cannot be both the direct result of some underlying thermodynamic or structural correlations.

A decoupling between dynamic and static correlation length scales has been reported before in computer simulations.^{43,89} For the present 2D model in particular, a comparison between the static point-to-set length scale^{54,55,90} and the average chord length confirmed this suggestion.⁴³ Therefore, we extract the point-to-set length from the literature for our 2D system²⁰ and compare it to the dynamic length scales in Figure 10a. This comparison confirms the observation that dynamic length scales from the physical MC dynamics are decoupled from the static point-to-set length scale. Interestingly, our results in Figure 10a indicate that the growth of the dynamic length scale characterizing the SMC dynamics very closely resembles the evolution of the point-to-set length scale.

We now perform a similar analysis for the 3D system in Figure 10b, but we have fewer literature results to guide our analysis. First, no alternative measurement of the dynamic correlation length scale is available for the 3D system studied here. However, our own data are sufficient to conclude, as for the 2D system, that the SMC dynamic correlation length scale is smaller and grows more slowly than the one characterizing the MC dynamics. Regarding static correlations, the point-to-set correlation length scale has not been measured for our 3D system of polydisperse soft spheres. However, the configurational entropy $S_{\text{conf}}(T)$ has been estimated,⁹¹ which can be used to infer the point-to-set length scale as $(TS_{\text{conf}})^{-2/3}$.^{24,53} We add this estimate in Figure 10b, using an arbitrary vertical shift to convert this number to a physical length scale with a behavior compatible with known results for the point-to-set length scale for similar systems.²⁴ Despite these caveats, we again find that, for the 3D system, the point-to-set length scale is strongly decoupled from the dynamic correlation length scale for the MC dynamics but is more strongly correlated with the one characterizing the SMC dynamics.

V.C. Adam–Gibbs Relation. The observation that MC and SMC dynamic correlation length scales are respectively decoupled and coupled to numerical estimates of static correlation length scales encourages us to revisit the Adam–Gibbs relation⁹² that connects the configurational entropy to the bulk relaxation time. This relation was first formulated by Adam and Gibbs in order to infer a dynamic slowing down from a decreasing configurational entropy, which had been noticed by Kauzmann.⁹³ The formula was then revisited and incorporated in the more modern framework of the random first-order transition (RFOT) theory,⁹⁴ and, in particular, in its phenomenological extension to finite dimensions.^{53,54}

In this view, the Adam–Gibbs relation is the mathematical formulation of the physical statement that the sharp decrease of the configurational entropy $S_{\text{conf}}(T)$ is causally responsible for the rapid growth of the bulk relaxation time $\tau_a(T)$ as the temperature decreases toward the glass transition:

$$\log\left(\frac{\tau_\alpha}{\tau_o}\right) \propto \frac{1}{TS_{\text{conf}}} \quad (8)$$

where τ_o is a microscopic time scale, roughly corresponding to the value of the structural relaxation time at the onset temperature. Several numerical^{95–97} and experimental^{1,98} studies have tested the validity of this relation.

We investigate if and how this relation is obeyed for the two types of dynamics studied here for the same models. By construction, the right-hand side of eq 8 is a purely thermodynamic quantity, while the left-hand side depends on the microscopic dynamics. A test of the Adam–Gibbs relation amounts to a parametric plot of the relation between τ_α and S_{conf} using temperature as a running parameter (see Figure 11). For the quantity τ_o , we use the value of τ_α of our dynamics

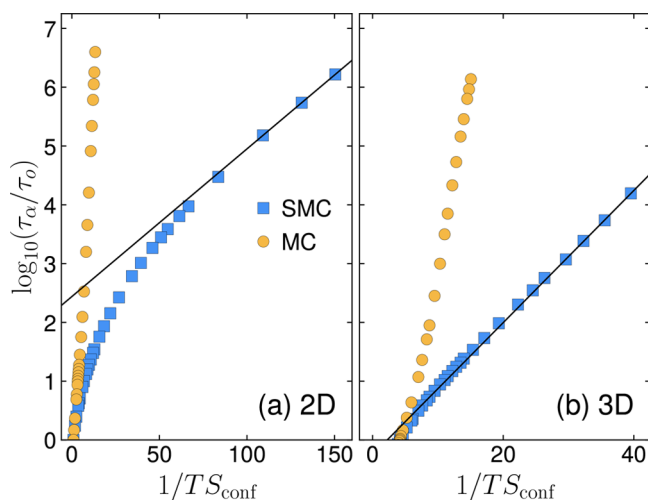


Figure 11. Adam–Gibbs plots for SMC and MC dynamics in (a) 2D and (b) 3D. Black lines represent the Adam–Gibbs relation (eq 8) fitted from SMC data at low temperatures.

data at the onset temperature T_o , as determined in ref 58. ($T_o = 1.006$ in 2D and $T_o = 0.266$ in 3D.) For S_{conf} , we use the fits to the data obtained in ref 58.

Over the limited time window allowed by the simulations, we find an apparent linear relation between $\log(\tau_\alpha)$ and $1/TS_{\text{conf}}$ in good agreement with eq 8. This was noticed previously for the present models in the context of MC dynamics,⁵⁸ as well as in many other models.⁹⁹ Interestingly, we find that the SMC dynamics also obeys the Adam–Gibbs relation in the low-temperature regime. Together with the observation that the SMC dynamic correlation length scale is comparable to the point-to-set length scale (while the MC one is not), this suggests that the SMC dynamics in fact obeys more closely the physical picture predicted by RFOT theory and captured by the Adam–Gibbs relation.

Pushing this line of thought to its limit, we can use the results in ref 58 regarding the relation between entropy and point-to-set length scale to infer numerical values for the dynamic exponent ψ that expresses the relation between τ_α and the point-to-set length scale. For the SMC dynamics, we obtain by this reasoning the value $\psi \approx 0.9$ in 2D and $\psi \approx 1.2–1.7$ for 3D. Although these estimates are of course limited by the modest time window accessible to the simulations, they are fully compatible with the predicted range $\psi \in [d/2, d]$, whereas the MC results are usually less satisfactory and lead to

quite small values of ψ , especially in 3D where $\psi = 0.75–0.9$ was found for MC dynamics.⁵⁸ (See ref 100 for an experimental counterpart to the latter finding.)

As a final note, we remark that testing the validity of the Adam–Gibbs relation by a parametric plot of $\log(\tau_\alpha)$ against S_{conf} is not easy, as the data often appear strongly correlated and are nearly linearly related. This is illustrated in Figure 11 where the two dynamics appear to satisfy the Adam–Gibbs relation reasonably well, which seems to be contradictory. A much stronger test of the connection between statics and dynamics is the strong correlation of dynamic and static length scales, as in Figure 10, which more directly probes the underlying physics. This issue is discussed further in the final section.

VI. ARE SWAP AND PHYSICAL DYNAMICS CORRELATED?

VI.A. Maps of Isoconfigurational Relaxation. So far, the comparison between MC and SMC dynamics established many differences: the relaxation times are different, the heterogeneity of the single-particle dynamics is different, and spatial correlations of the dynamics and links to thermodynamic fluctuations also differ.

These results may appear surprising, given the long line of research that has tried to establish deep connections between structure and dynamics in supercooled liquids.^{101–104} How can the same structure be a good predictor of two widely different dynamics? To address this question, it is useful to raise an intermediate point and ask how strongly MC and SMC dynamics are correlated to each other.

We directly compared maps of local relaxation dynamics produced by MC and SMC, and their relation to the underlying structure of the supercooled liquid. To do so, we use the isoconfigurational ensemble¹⁰⁵ and run a large number of trajectories using either MC or SMC starting from the same initial condition. In practice, we first prepare equilibrium configurations by using the SMC algorithm. Starting from each configuration, we perform both MC and SMC simulations. Trajectories are generated by using different sets of random numbers. In both cases, the number of isoconfigurational trajectories is 400. We characterize the local relaxation by the self-intermediate scattering function measured for each particle: $f_s^i(q, t) = \cos(q \cdot \Delta r_i^{\text{CR}}(t))$.

To get a qualitative feeling for the degree of correlation between MC and SMC isoconfigurational dynamics, we show, in Figure 12, an example of a map of isoconfigurationally averaged local relaxation functions for the same initial condition but by using the two dynamics. We choose the temperature $T = 0.130$ in 2D, where the MC dynamics is already glassy ($\tau_\alpha = 2.0 \times 10^7$), but SMC dynamics is rather fast ($\tau_\alpha = 4.5 \times 10^3$). Both maps are taken at the respective τ_α . The MC map in Figure 12a displays a clear spatial separation between relaxed (red) regions and unrelaxed (blue) ones, thus revealing spatially extended dynamic correlations and a large dynamic correlation length scale. For this particular system, this heterogeneous pattern is known to be largely controlled by dynamic facilitation,^{43,44} but it also correlates with various structural quantities.^{106–109}

The SMC map in Figure 12b is strikingly different. The dynamic contrast between relaxed and unrelaxed regions is suppressed, while the spatial extension of dynamic correlations is also much smaller. These observations offer microscopic support to the suppression of single-particle heterogeneity

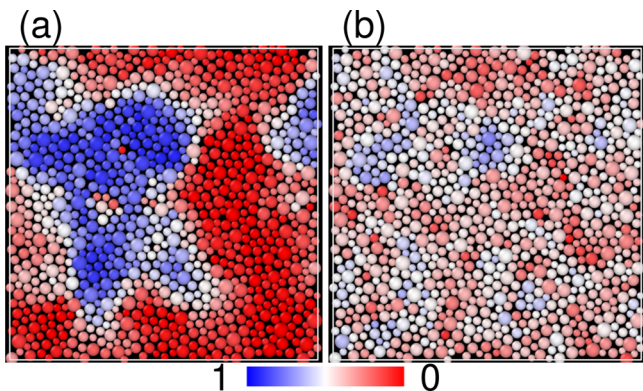


Figure 12. Isoconfigurational relaxation maps in (a) MC and (b) SMC dynamics at $T = 0.130$ starting from the same initial condition. Both panels show configurations at $\tau_\alpha = 2.0 \times 10^7$ in panel (a) and $\tau_\alpha = 4.5 \times 10^3$ in panel (b).

discussed in **Section IV** and of collective relaxations in **Section V**.

Looking more carefully in the SMC map, we do observe some spatial heterogeneity, revealing, for instance, bluer regions that are more stable than average. For instance, the top left corner has more blue particles, which seems reminiscent of the large blue region that appears in the MC map. This may indicate that structurally stable regions influence both dynamics but give rise to distinct dynamic heterogeneity patterns.

VI.B. Correlation between the Two Dynamics. To quantify the similarity between MC and SMC isoconfigurational relaxation maps, we introduce the following Pearson correlation coefficient:

$$\rho_p(\mathbf{x}(t_{\text{MC}}), \mathbf{y}(t_{\text{SMC}})) = \frac{\sum_i \delta x_i \delta y_i}{\sqrt{\sum_i \delta x_i^2} \sqrt{\sum_i \delta y_i^2}} \quad (9)$$

This is valid between the vector $\mathbf{x} = (f_s^1(q, t_{\text{MC}}), \dots, f_s^N(q, t_{\text{MC}}))$ of local relaxation in the MC isoconfigurational ensemble, and that of the SMC ensemble, $\mathbf{y} = (f_s^1(q, t_{\text{SMC}}), \dots, f_s^N(q, t_{\text{SMC}}))$, with $\delta x = x - \langle x \rangle$ being the deviation from the average. In the calculation of the Pearson coefficient, we averaged over five independent initial configurations.

Since the Pearson coefficient depends on the times chosen in each dynamics to quantify the local dynamics, we present, in **Figure 13**, a heat map of its evolution with both quantities t_{MC} and t_{SMC} , where the relaxation times τ_α are indicated with black lines. The correlation between both dynamics is maximal at very short times with a large Pearson correlation ($\rho_p > 0.97$). This is reasonable, since, at short times, swap moves have very little influence on the dynamics. However, the correlation degrades rapidly as times grow toward the structural relaxation times, to reach $\rho_p \approx 0.4$ at τ_α . The modest degree of correlation rationalizes the above observations regarding the important differences in various signatures of glassy dynamics. We also note that, although modest, the correlation is not vanishing (the Pearson coefficient is zero for uncorrelated variables), suggesting the possibility that some underlying structural features can indeed be predictors of both dynamics. It would be useful to apply, for instance, machine learning tools used to predict the MC dynamics to also predict the SMC one.

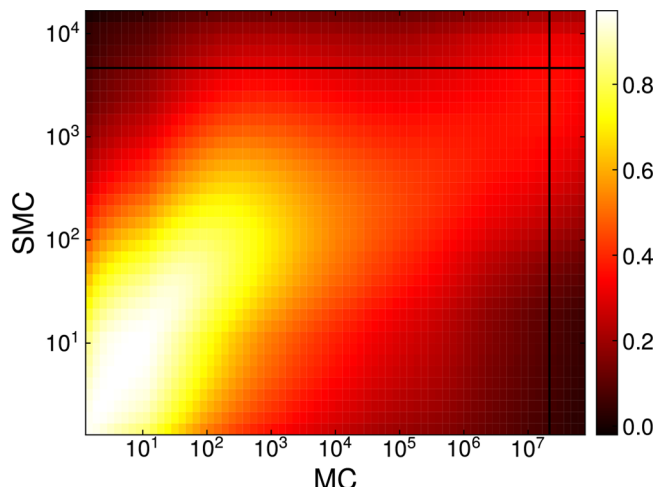


Figure 13. Pearson correlation coefficient between MC dynamics at time t_{MC} and SMC dynamics at time t_{SMC} . The black lines correspond to the structural relaxation time τ_α in the MC and SMC dynamics, respectively.

VII. DISCUSSION

We have performed extensive simulations of two glass-forming liquids to offer a detailed comparison between SMC dynamics and conventional MC. In addition to the known acceleration of the bulk dynamics, we have discovered a strong suppression of dynamic heterogeneity, with a smaller contrast between fast and slow particles, together with a drastic shortening of spatial correlations of the dynamics. We also showed that even when comparing MC and SMC on a more equal footing using plots parametrized by the growing relaxation time, the strong suppression of dynamic heterogeneity persists.

A central numerical result is the relation between the growth of spatial correlations of the dynamics, which is different from observations using conventional MC. However, the decoupling between dynamic and static fluctuations observed for MC is also very much suppressed in SMC, and the behavior of dynamic correlations in SMC is very similar to measurements of static correlations. The growth of the point-to-set correlation length scale is similar to the one of the SMC dynamic correlation length scale, the Adam–Gibbs relation is satisfied with reasonable values of the dynamic exponent ψ .

Let us now turn to a physical interpretation of these results. We first recall that although it is nonphysical, in the sense that swap moves do not appear during the conventional MC or MD dynamics, the SMC dynamics can nevertheless be seen as a local dynamics, in which the diameters are now fluctuating quantities.¹⁹ As such, it represents valid microscopic dynamics that can in principle be studied using theoretical tools similar to the MD dynamics. It is thus a totally valid question to ask about its physical interpretation and relation to available theoretical approaches to glass transition dynamics.

It was proposed, in particular, that SMC dynamics corresponds to an ordinary glassy dynamics, but with a mode-coupling crossover temperature that it is depressed to lower temperatures.^{50–52} We find no strong evidence from the numerical simulations for this interpretation, beyond the obvious fact that the temperature dependence of the bulk relaxation time is indeed shifted to lower temperatures, as shown in **Figure 2**. The observation of suppressed deviations from non-Gaussian dynamic behavior coupled to a growth of the dynamic susceptibility maybe reminiscent of the reported

behavior found in the Gaussian core model,^{110,111} which was indeed interpreted as a model behaving more closely according to the predictions of the mode-coupling theory of the glass transition. This interpretation is difficult to reconcile with the lack of a clear power-law description of the growth of τ_α within SMC, and the strong correlation with static correlations, which suggests that dynamics should be better described by invoking thermally activated processes.

A more logical interpretation of the numerical results is that the swap Monte Carlo moves, by introducing stronger fluctuations at the local scale (leading, for instance, to enhanced vibrational motion at short times¹⁹), effectively reduce the influence of local kinetic constraints that contribute to the slowdown of the physical MC dynamics. As a result, the SMC dynamic heterogeneity becomes less pronounced. The observation that dynamic correlations are spatially less extended than in MC also suggests that dynamic facilitation must be much less relevant for SMC dynamics, a suggestion that should be confirmed in future work using, for instance, the approach of refs 43 and 44. This interpretation is also consistent with a recent work emphasizing the role of local kinetic constraints on glassy dynamics.⁴⁷ Our conclusions are also consistent with the ones obtained from the study of a kinetically constrained model.⁴⁸

For the two polydisperse models considered here, where swap Monte Carlo is extremely efficient, the dynamic correlation length scale of the SMC dynamics seems very close to the point-to-set length scale, while the Adam–Gibbs relation is obeyed. Our interpretation is that the suppression of local barriers is so efficient in these two models that the activated dynamics involving collective rearrangements of particles over a length scale given by the point-to-set length scale is at play, following the finite dimensional predictions of the RFOT theory. A logical corollary is that RFOT theory does not describe well the physical MC dynamics.^{46,47} In future work, one should also test this interpretation, for instance by comparing the dynamic correlations revealed by the SMC dynamics to the spatial fluctuations of the static Franz–Parisi potential measured in ref 112, or the local fluctuations of the configurational entropy.¹¹³

The rigorous relations between time scales and length scales discussed in ref 55, together with the correlation between SMC dynamics and static fluctuations, suggest that, for these polydisperse models, local barriers are so efficiently suppressed that the slowdown of the SMC dynamics at low temperature is mostly controlled by the growth of the point-to-set length scale, and thus ultimately, by the approach to a random first-order transition, akin to a Kauzmann transition at temperature T_K . This would, for instance, explain the extreme acceleration of the dynamics in 2D where $T_K \approx 0$.²⁰ A direct consequence of this interpretation, however, is that, for these models no local Monte Carlo algorithm will be able to improve much the performances of the SMC algorithm. This suggests that future algorithms to equilibrate supercooled liquids even faster should be able to perform collective Monte Carlo that can effectively lower the value of the dynamic exponent ψ . For this, alternatives to the SMC algorithm should be developed that involve more collective moves^{13,14,114,115} or nonequilibrium approaches.¹¹⁶

AUTHOR INFORMATION

Corresponding Author

Ludovic Berthier – Laboratoire Charles Coulomb (L2C), Université de Montpellier, CNRS, 34095 Montpellier, France; Gulliver, UMR CNRS 7083, ESPCI Paris, PSL Research University, 75005 Paris, France;  orcid.org/0000-0003-2059-702X; Email: ludovic.berthier@espci.fr

Author

Kumpei Shiraishi – Laboratoire Charles Coulomb (L2C), Université de Montpellier, CNRS, 34095 Montpellier, France;  orcid.org/0000-0002-6998-2319

Complete contact information is available at:
<https://pubs.acs.org/10.1021/acs.jpcb.4c06702>

Notes

The authors declare no competing financial interest.

ACKNOWLEDGMENTS

We thank Misaki Ozawa, Cecilia Herrero, Camille Scalliet, Hayato Shiba, Matthieu Wyart for sharing their data and for valuable discussions. This work is supported by the Japan Society for the Promotion of Science (JSPS), through the Overseas Research Fellowships (K.S.).

REFERENCES

- (1) Ediger, M. D.; Angell, C. A.; Nagel, S. R. Supercooled Liquids and Glasses. *J. Phys. Chem.* **1996**, *100*, 13200–13212.
- (2) Berthier, L.; Biroli, G. Theoretical perspective on the glass transition and amorphous materials. *Rev. Mod. Phys.* **2011**, *83*, 587–645.
- (3) Berthier, L.; Reichman, D. R. Modern computational studies of the glass transition. *Nat. Rev. Phys.* **2023**, *5*, 102–116.
- (4) Frenkel, D., Smit, B. *Understanding Molecular Simulation*; Academic Press, 2002.
- (5) Allen, M. P., Tildesley, D. J. *Computer Simulation of Liquids*; Oxford University Press, 2017.
- (6) Berthier, L.; Kob, W. The Monte Carlo dynamics of a binary Lennard-Jones glass-forming mixture. *J. Phys.: Condens. Matter* **2007**, *19*, 205130.
- (7) Barrat, J.-L.; Berthier, L. Computer simulations of the glass transition and glassy materials. *Comp. Rend. Phys.* **2023**, *24*, 57–73.
- (8) Hukushima, K.; Nemoto, K. Exchange Monte Carlo Method and Application to Spin Glass Simulations. *J. Phys. Soc. Jpn.* **1996**, *65*, 1604–1608.
- (9) Yamamoto, R.; Kob, W. Replica-exchange molecular dynamics simulation for supercooled liquids. *Phys. Rev. E* **2000**, *61*, 5473.
- (10) Jung, G.; Biroli, G.; Berthier, L. Normalizing flows as an enhanced sampling method for atomistic supercooled liquids. *Machine Learning: Sci. Technol.* **2024**, *5*, 035053.
- (11) Bernard, E. P.; Krauth, W.; Wilson, D. B. Event-chain Monte Carlo algorithms for hard-sphere systems. *Phys. Rev. E* **2009**, *80*, 056704.
- (12) Isobe, M.; Keys, A. S.; Chandler, D.; Garrahan, J. P. Applicability of Dynamic Facilitation Theory to Binary Hard Disk Systems. *Phys. Rev. Lett.* **2016**, *117*, 145701.
- (13) Ghimenti, F.; Berthier, L.; van Wijland, F. Irreversible Monte Carlo Algorithms for Hard Disk Glasses: From Event-Chain to Collective Swaps. *Phys. Rev. Lett.* **2024**, *133*, 028202.
- (14) Berthier, L.; Ghimenti, F.; van Wijland, F. Monte Carlo simulations of glass-forming liquids beyond Metropolis. *J. Chem. Phys.* **2024**, *161*, 114105.
- (15) Ciarella, S.; Trinquier, J.; Weigt, M.; Zamponi, F. Machine-learning-assisted Monte Carlo fails at sampling computationally hard problems. *Machine Learning: Sci. Technol.* **2023**, *4*, 010501.

- (16) Kranendonk, W.; Frenkel, D. Computer simulation of solid-liquid coexistence in binary hard sphere mixtures. *Mol. Phys.* **1991**, *72*, 679–697.
- (17) Grigera, T. S.; Parisi, G. Fast Monte Carlo algorithm for supercooled soft spheres. *Phys. Rev. E* **2001**, *63*, 045102.
- (18) Berthier, L.; Coslovich, D.; Ninarello, A.; Ozawa, M. Equilibrium Sampling of Hard Spheres up to the Jamming Density and Beyond. *Phys. Rev. Lett.* **2016**, *116*, 238002.
- (19) Ninarello, A.; Berthier, L.; Coslovich, D. Models and Algorithms for the Next Generation of Glass Transition Studies. *Phys. Rev. X* **2017**, *7*, 021039.
- (20) Berthier, L.; Charbonneau, P.; Ninarello, A.; Ozawa, M.; Yaida, S. Zero-temperature glass transition in two dimensions. *Nat. Commun.* **2019**, *10*, 1508.
- (21) Fullerton, C. J.; Berthier, L. Glassy Behavior of Sticky Spheres: What Lies beyond Experimental Timescales? *Phys. Rev. Lett.* **2020**, *125*, 258004.
- (22) Parmar, A. D. S.; Ozawa, M.; Berthier, L. Ultrastable Metallic Glasses In Silico. *Phys. Rev. Lett.* **2020**, *125*, 050502.
- (23) Jung, G.; Biroli, G.; Berthier, L. Predicting Dynamic Heterogeneity in Glass-Forming Liquids by Physics-Inspired Machine Learning. *Phys. Rev. Lett.* **2023**, *130*, 238202.
- (24) Berthier, L.; Charbonneau, P.; Coslovich, D.; Ninarello, A.; Ozawa, M.; Yaida, S. Configurational entropy measurements in extremely supercooled liquids that break the glass ceiling. *Proc. Natl. Acad. Sci. U. S. A.* **2017**, *114*, 11356–11361.
- (25) Guiselin, B.; Berthier, L.; Tarjus, G. Statistical mechanics of coupled supercooled liquids in finite dimensions. *SciPost Phys.* **2022**, *12*, 091.
- (26) Ozawa, M.; Berthier, L.; Biroli, G.; Rosso, A.; Tarjus, G. Random critical point separates brittle and ductile yielding transitions in amorphous materials. *Proc. Natl. Acad. Sci. U. S. A.* **2018**, *115*, 6656–6661.
- (27) Richard, D.; et al. Predicting plasticity in disordered solids from structural indicators. *Phys. Rev. Mater.* **2020**, *4*, 113609.
- (28) Wang, L.; Ninarello, A.; Guan, P.; Berthier, L.; Szamel, G.; Flenner, E. Low-frequency vibrational modes of stable glasses. *Nat. Commun.* **2019**, *10*, 26.
- (29) Khomenko, D.; Scalliet, C.; Berthier, L.; Reichman, D. R.; Zamponi, F. Depletion of Two-Level Systems in Ultrastable Computer-Generated Glasses. *Phys. Rev. Lett.* **2020**, *124*, 225901.
- (30) Mocanu, F. C.; Berthier, L.; Ciarella, S.; Khomenko, D.; Reichman, D. R.; Scalliet, C.; Zamponi, F. Microscopic observation of two-level systems in a metallic glass model. *J. Chem. Phys.* **2023**, *158*, 014501.
- (31) Swallen, S. F.; Kearns, K. L.; Mapes, M. K.; Kim, Y. S.; McMahon, R. J.; Ediger, M. D.; Wu, T.; Yu, L.; Satija, S. Organic Glasses with Exceptional Thermodynamic and Kinetic Stability. *Science* **2007**, *315*, 353–356.
- (32) Ediger, M. D. Perspective: Highly stable vapor-deposited glasses. *J. Chem. Phys.* **2017**, *147*, 210901.
- (33) Berthier, L.; Charbonneau, P.; Flenner, E.; Zamponi, F. Origin of Ultrastability in Vapor-Deposited Glasses. *Phys. Rev. Lett.* **2017**, *119*, 188002.
- (34) Berthier, L.; Ediger, M. D. How to “measure” a structural relaxation time that is too long to be measured? *J. Chem. Phys.* **2020**, *153*, 044501.
- (35) Herrero, C.; Scalliet, C.; Ediger, M. D.; Berthier, L. Two-step devitrification of ultrastable glasses. *Proc. Natl. Acad. Sci. U. S. A.* **2023**, *120*, e2220824120.
- (36) Herrero, C.; Ediger, M. D.; Berthier, L. Front propagation in ultrastable glasses is dynamically heterogeneous. *J. Chem. Phys.* **2023**, *159*, 114504.
- (37) Guiselin, B.; Scalliet, C.; Berthier, L. Microscopic origin of excess wings in relaxation spectra of supercooled liquids. *Nat. Phys.* **2022**, *18*, 468–472.
- (38) Ediger, M. D. Spatially Heterogeneous Dynamics in Supercooled Liquids. *Annu. Rev. Phys. Chem.* **2000**, *51*, 99–128.
- (39) Donati, C.; Glotzer, S. C.; Poole, P. H. Growing Spatial Correlations of Particle Displacements in a Simulated Liquid on Cooling toward the Glass Transition. *Phys. Rev. Lett.* **1999**, *82*, 5064.
- (40) Berthier, L.; Biroli, G.; Bouchaud, J.-P.; Cipelletti, L.; van Saarloos, W., Eds., *Dynamical Heterogeneities in Glasses, Colloids, and Granular Media*; Oxford University Press, 2011.
- (41) Keys, A. S.; Garrahan, J. P.; Chandler, D. Calorimetric glass transition explained by hierarchical dynamic facilitation. *Proc. Natl. Acad. Sci. U. S. A.* **2013**, *110*, 4482–4487.
- (42) Chandler, D.; Garrahan, J. P. Dynamics on the Way to Forming Glass: Bubbles in Space-Time. *Annu. Rev. Phys. Chem.* **2010**, *61*, 191–217.
- (43) Scalliet, C.; Guiselin, B.; Berthier, L. Thirty Milliseconds in the Life of a Supercooled Liquid. *Phys. Rev. X* **2022**, *12*, 041028.
- (44) Herrero, C.; Berthier, L. Direct Numerical Analysis of Dynamic Facilitation in Glass-Forming Liquids. *Phys. Rev. Lett.* **2024**, *132*, 258201.
- (45) Chacko, R. N.; Landes, F. P.; Biroli, G.; Dauchot, O.; Liu, A. J.; Reichman, D. R. Dynamical Facilitation Governs the Equilibration Dynamics of Glasses. *Phys. Rev. X* **2024**, *14*, 031012.
- (46) Wyart, M.; Cates, M. E. Does a Growing Static Length Scale Control the Glass Transition? *Phys. Rev. Lett.* **2017**, *119*, 195501.
- (47) Gavazzoni, C.; Brito, C.; Wyart, M. Testing Theories of the Glass Transition with the Same Liquid but Many Kinetic Rules. *Phys. Rev. Lett.* **2024**, *132*, 248201.
- (48) Gutiérrez, R.; Garrahan, J. P.; Jack, R. L. Accelerated relaxation and suppressed dynamic heterogeneity in a kinetically constrained (East) model with swaps. *J. Stat. Mech.: Theory Exp.* **2019**, *2019*, 094006.
- (49) Berthier, L.; Biroli, G.; Bouchaud, J.-P.; Tarjus, G. Can the glass transition be explained without a growing static length scale? *J. Chem. Phys.* **2019**, *150*, 094501.
- (50) Ikeda, H.; Zamponi, F.; Ikeda, A. Mean field theory of the swap Monte Carlo algorithm. *J. Chem. Phys.* **2017**, *147*, 234506.
- (51) Szamel, G. Theory for the dynamics of glassy mixtures with particle size swaps. *Phys. Rev. E* **2018**, *98*, 050601.
- (52) Brito, C.; Lerner, E.; Wyart, M. Theory for Swap Acceleration near the Glass and Jamming Transitions for Continuously Polydisperse Particles. *Phys. Rev. X* **2018**, *8*, 031050.
- (53) Kirkpatrick, T. R.; Thirumalai, D.; Wolynes, P. G. Scaling concepts for the dynamics of viscous liquids near an ideal glassy state. *Phys. Rev. A* **1989**, *40*, 1045.
- (54) Bouchaud, J.-P.; Biroli, G. On the Adam-Gibbs-Kirkpatrick-Thirumalai-Wolynes scenario for the viscosity increase in glasses. *J. Chem. Phys.* **2004**, *121*, 7347–7354.
- (55) Montanari, A.; Semerjian, G. Rigorous Inequalities Between Length and Time Scales in Glassy Systems. *J. Stat. Phys.* **2006**, *125*, 23–54.
- (56) Mazoyer, S.; Ebert, F.; Maret, G.; Keim, P. Dynamics of particles and cages in an experimental 2D glass former. *Europhys. Lett.* **2009**, *88*, 66004.
- (57) Illing, B.; Fritsch, S.; Kaiser, H.; Klix, C. L.; Maret, G.; Keim, P. Mermin–Wagner fluctuations in 2D amorphous solids. *Proc. Natl. Acad. Sci. U. S. A.* **2017**, *114*, 1856–1861.
- (58) Ozawa, M.; Scalliet, C.; Ninarello, A.; Berthier, L. Does the Adam-Gibbs relation hold in simulated supercooled liquids? *J. Chem. Phys.* **2019**, *151*, 084504.
- (59) Berthier, L.; Flenner, E.; Fullerton, C. J.; Scalliet, C.; Singh, M. Efficient swap algorithms for molecular dynamics simulations of equilibrium supercooled liquids. *J. Stat. Mech.: Theory Exp.* **2019**, *2019*, 064004.
- (60) Götze, W. *Complex Dynamics of Glass-Forming Liquids: A Mode-Coupling Theory*; Oxford University Press, 2008.
- (61) Kühler, N.; Horbach, J. Understanding the swap Monte Carlo algorithm in a size-polydisperse model glassformer. *Phys. Rev. E* **2023**, *108*, 024127.
- (62) Berthier, L.; Biroli, G.; Bouchaud, J.-P.; Kob, W.; Miyazaki, K.; Reichman, D. R. Spontaneous and induced dynamic fluctuations in

- glass formers. I. General results and dependence on ensemble and dynamics. *J. Chem. Phys.* **2007**, *126*, 184503.
- (63) Kob, W.; Donati, C.; Plimpton, S. J.; Poole, P. H.; Glotzer, S. C. Dynamical Heterogeneities in a Supercooled Lennard-Jones Liquid. *Phys. Rev. Lett.* **1997**, *79*, 2827.
- (64) Chaudhuri, P.; Berthier, L.; Kob, W. Universal Nature of Particle Displacements close to Glass and Jamming Transitions. *Phys. Rev. Lett.* **2007**, *99*, 060604.
- (65) Berthier, L.; Flennier, E.; Szamel, G. Comment on “Fickian Non-Gaussian Diffusion in Glass-Forming Liquids. *Phys. Rev. Lett.* **2023**, *131*, 119801.
- (66) Rahman, A. Correlations in the Motion of Atoms in Liquid Argon. *Phys. Rev.* **1964**, *136*, A405–A411.
- (67) Biroli, G.; Charbonneau, P.; Folena, G.; Hu, Y.; Zamponi, F. Local Dynamical Heterogeneity in Simple Glass Formers. *Phys. Rev. Lett.* **2022**, *128*, 175501.
- (68) Flennier, E.; Szamel, G. Relaxation in a glassy binary mixture: Mode-coupling-like power laws, dynamic heterogeneity, and a new non-Gaussian parameter. *Phys. Rev. E* **2005**, *72*, 011205.
- (69) Cicerone, M. T.; Ediger, M. D. Enhanced translation of probe molecules in supercooled *o*-terphenyl: Signature of spatially heterogeneous dynamics? *J. Chem. Phys.* **1996**, *104*, 7210.
- (70) Swallen, S. F.; Bonvallet, P. A.; McMahon, R. J.; Ediger, M. D. Self-Diffusion of tris-Naphthylbenzene near the Glass Transition Temperature. *Phys. Rev. Lett.* **2003**, *90*, 015901.
- (71) Tarjus, G.; Kivelson, D. Breakdown of the Stokes–Einstein relation in supercooled liquids. *J. Chem. Phys.* **1995**, *103*, 3071.
- (72) Berthier, L. Time and length scales in supercooled liquids. *Phys. Rev. E* **2004**, *69*, 020201.
- (73) Kumar, S. K.; Szamel, G.; Douglas, J. F. Nature of the breakdown in the Stokes–Einstein relationship in a hard sphere fluid. *J. Chem. Phys.* **2006**, *124*, 214501.
- (74) Eaves, J. D.; Reichman, D. R. Spatial dimension and the dynamics of supercooled liquids. *Proc. Natl. Acad. Sci. U. S. A.* **2009**, *106*, 15171–15175.
- (75) Parmar, A. D. S.; Sengupta, S.; Sastry, S. Length-Scale Dependence of the Stokes–Einstein and Adam–Gibbs Relations in Model Glass Formers. *Phys. Rev. Lett.* **2017**, *119*, 056001.
- (76) Kawasaki, T.; Kim, K. Identifying time scales for violation/preservation of Stokes–Einstein relation in supercooled water. *Sci. Adv.* **2017**, *3*, e1700399.
- (77) Das, P.; Sastry, S. Crossover in dynamics in the Kob-Andersen binary mixture glass-forming liquid. *J. Non-Cryst. Solids: X* **2022**, *14*, 100098.
- (78) Berthier, L.; Chandler, D.; Garrahan, J. P. Length scale for the onset of Fickian diffusion in supercooled liquids. *Europhys. Lett.* **2005**, *69*, 320–326.
- (79) Shiba, H.; Kawasaki, T.; Kim, K. Local Density Fluctuation Governs the Divergence of Viscosity Underlying Elastic and Hydrodynamic Anomalies in a 2D Glass-Forming Liquid. *Phys. Rev. Lett.* **2019**, *123*, 265501.
- (80) Li, Y.-W.; Mishra, C. K.; Sun, Z.-Y.; Zhao, K.; Mason, T. G.; Ganapathy, R.; Pica Ciamarra, M. Long-wavelength fluctuations and anomalous dynamics in 2-dimensional liquids. *Proc. Natl. Acad. Sci. U. S. A.* **2019**, *116*, 22977–22982.
- (81) Karmakar, S.; Dasgupta, C.; Sastry, S. Growing Length Scales and Their Relation to Timescales in Glass-Forming Liquids. *Ann. Rev. Condensed Matter Phys.* **2014**, *5*, 255–284.
- (82) Franz, S.; Donati, C.; Parisi, G.; Glotzer, S. C. On dynamical correlations in supercooled liquids. *Philos. Mag. B* **1999**, *79*, 1827–1831.
- (83) Glotzer, S. C.; Novikov, V. N.; Schröder, T. B. Time-dependent, four-point density correlation function description of dynamical heterogeneity and decoupling in supercooled liquids. *J. Chem. Phys.* **2000**, *112*, 509–512.
- (84) Laćević, N.; Starr, F. W.; Schröder, T. B.; Glotzer, S. C. Spatially heterogeneous dynamics investigated via a time-dependent four-point density correlation function. *J. Chem. Phys.* **2003**, *119*, 7372–7387.
- (85) Toninelli, C.; Wyart, M.; Berthier, L.; Birol, G.; Bouchaud, J.-P. Dynamical susceptibility of glass formers: Contrasting the predictions of theoretical scenarios. *Phys. Rev. E* **2005**, *71*, 041505.
- (86) Karmakar, S.; Dasgupta, C.; Sastry, S. Growing length and time scales in glass-forming liquids. *Proc. Natl. Acad. Sci. U. S. A.* **2009**, *106*, 3675–3679.
- (87) Coslovich, D.; Ozawa, M.; Kob, W. Dynamic and thermodynamic crossover scenarios in the Kob-Andersen mixture: Insights from multi-CPU and multi-GPU simulations. *Eur. Phys. J. E* **2018**, *41*, 62.
- (88) Ortlieb, L.; Ingebrigtsen, T. S.; Hallett, J. E.; Turci, F.; Royall, C. P. Probing excitations and cooperatively rearranging regions in deeply supercooled liquids. *Nat. Commun.* **2023**, *14*, 2621.
- (89) Charbonneau, P.; Tarjus, G. Decorrelation of the static and dynamic length scales in hard-sphere glass formers. *Phys. Rev. E* **2013**, *87*, 042305.
- (90) Birol, G.; Bouchaud, J.-P.; Cavagna, A.; Grigera, T. S.; Verrocchio, P. Thermodynamic signature of growing amorphous order in glass-forming liquids. *Nat. Phys.* **2008**, *4*, 771–775.
- (91) Ozawa, M.; Parisi, G.; Berthier, L. Configurational entropy of polydisperse supercooled liquids. *J. Chem. Phys.* **2018**, *149*, 154501.
- (92) Adam, G.; Gibbs, J. H. On the Temperature Dependence of Cooperative Relaxation Properties in Glass-Forming Liquids. *J. Chem. Phys.* **1965**, *43*, 139.
- (93) Kauzmann, W. The Nature of the Glassy State and the Behavior of Liquids at Low Temperatures. *Chem. Rev.* **1948**, *43*, 219–256.
- (94) Parisi, G.; Urbani, P.; Zamponi, F. *Theory of Simple Glasses: Exact Solutions in Infinite Dimensions*; Cambridge University Press, 2020.
- (95) Sastry, S. The relationship between fragility, configurational entropy and the potential energy landscape of glass-forming liquids. *Nature* **2001**, *409*, 164–167.
- (96) Sengupta, S.; Karmakar, S.; Dasgupta, C.; Sastry, S. Adam–Gibbs Relation for Glass-Forming Liquids in Two, Three, and Four Dimensions. *Phys. Rev. Lett.* **2012**, *109*, 095705.
- (97) Handle, P. H.; Sciortino, F. The Adam–Gibbs relation and the TIP4P/2005 model of water. *Mol. Phys.* **2018**, *116*, 3366–3371.
- (98) Richert, R.; Angell, C. A. Dynamics of glass-forming liquids. V. On the link between molecular dynamics and configurational entropy. *J. Chem. Phys.* **1998**, *108*, 9016.
- (99) Sastry, S. Liquid Limits: Glass Transition and Liquid–Gas Spinodal Boundaries of Metastable Liquids. *Phys. Rev. Lett.* **2000**, *85*, 590.
- (100) Capaccioli, S.; Ruocco, G.; Zamponi, F. Dynamically Correlated Regions and Configurational Entropy in Supercooled Liquids. *J. Phys. Chem. B* **2008**, *112*, 10652–10658.
- (101) Kawasaki, T.; Araki, T.; Tanaka, H. Correlation between Dynamic Heterogeneity and Medium-Range Order in Two-Dimensional Glass-Forming Liquids. *Phys. Rev. Lett.* **2007**, *99*, 215701.
- (102) Royall, C. P.; Williams, S. R. The role of local structure in dynamical arrest. *Phys. Rep.* **2015**, *560*, 1–75.
- (103) Hallett, J. E.; Turci, F.; Royall, C. P. Local structure in deeply supercooled liquids exhibits growing lengthscales and dynamical correlations. *Nat. Commun.* **2018**, *9*, 3272.
- (104) Tanaka, H.; Tong, H.; Shi, R.; Russo, J. Revealing key structural features hidden in liquids and glasses. *Nat. Rev. Phys.* **2019**, *1*, 333–348.
- (105) Widmer-Cooper, A.; Harrowell, P.; Fynewever, H. How Reproducible Are Dynamic Heterogeneities in a Supercooled Liquid? *Phys. Rev. Lett.* **2004**, *93*, 135701.
- (106) Widmer-Cooper, A.; Perry, H.; Harrowell, P.; Reichman, D. R. Irreversible reorganization in a supercooled liquid originates from localized soft modes. *Nat. Phys.* **2008**, *4*, 711–715.
- (107) Schoenholz, S. S.; Cubuk, E. D.; Sussman, D. M.; Kaxiras, E.; Liu, A. J. A structural approach to relaxation in glassy liquids. *Nat. Phys.* **2016**, *12*, 469–471.
- (108) Tong, H.; Tanaka, H. Revealing Hidden Structural Order Controlling Both Fast and Slow Glassy Dynamics in Supercooled Liquids. *Phys. Rev. X* **2018**, *8*, 011041.

- (109) Lerbinger, M.; Barbot, A.; Vandembroucq, D.; Patinet, S. Relevance of Shear Transformations in the Relaxation of Supercooled Liquids. *Phys. Rev. Lett.* **2022**, *129*, 195501.
- (110) Ikeda, A.; Miyazaki, K. Glass Transition of the Monodisperse Gaussian Core Model. *Phys. Rev. Lett.* **2011**, *106*, 015701.
- (111) Coslovich, D.; Ikeda, A.; Miyazaki, K. Mean-field dynamic criticality and geometric transition in the Gaussian core model. *Phys. Rev. E* **2016**, *93*, 042602.
- (112) Guiselin, B.; Tarjus, G.; Berthier, L. Static self-induced heterogeneity in glass-forming liquids: Overlap as a microscope. *J. Chem. Phys.* **2022**, *156*, 194503.
- (113) Berthier, L. Self-Induced Heterogeneity in Deeply Supercooled Liquids. *Phys. Rev. Lett.* **2021**, *127*, 088002.
- (114) Dress, C.; Krauth, W. Cluster algorithm for hard spheres and related systems. *J. Phys. A: Math. Gen.* **1995**, *28*, L597–L601.
- (115) Michel, M.; Kapfer, S. C.; Krauth, W. Generalized event-chain Monte Carlo: Constructing rejection-free global-balance algorithms from infinitesimal steps. *J. Chem. Phys.* **2014**, *140*, 054116.
- (116) Ghimenti, F.; Berthier, L.; Szamel, G.; van Wijland, F. Sampling Efficiency of Transverse Forces in Dense Liquids. *Phys. Rev. Lett.* **2023**, *131*, 257101.